Characterization of an energy dispersive X-ray fluorescence imaging system based on a Micropattern Gaseous Detector

A.L.M. Silva, C.D.R. Azevedo, C.A.B. Oliveira, J.M.F. Dos Santos, M.L. Carvalho, J.F.C.A. Veloso

PII: S0584-8547(11)00053-X
DOI: doi: 10.1016/j.sab.2011.03.002
Reference: SAB 4255

To appear in: *Spectrochimica Acta Part B: Atomic Spectroscopy*

Received date: 4 January 2011
Accepted date: 7 March 2011

Characterization of an energy dispersive X-ray fluorescence imaging system based on a Micropattern Gaseous Detector

A.L.M. Silva[a], C.D.R. Azevedo[a], C.A.B. Oliveira[a], J.M.F. Dos Santos[b], M.L. Carvalho[c], J.F.C.A. Veloso[a]

[a] *I3N - Physics Department, University of Aveiro, 3810-193, Aveiro, Portugal*
[b] *Physics Department, University of Coimbra, 3004-516, Coimbra, Portugal*
[c] *Atomic Physics Centre, University of Lisbon, 1649-003 Lisboa, Portugal*

Abstract

An Energy Dispersive X-ray Fluorescence (EDXRF) imaging system based on a Micropattern Gas Detector has already shown good results for different applications. An X-ray tube, a pinhole camera and a Micro-Hole and Strip Plate (MHSP) based detector are the main components of the experimental system. The detector uses an MHSP in a Xe atmosphere at 1 bar, acting as a photon counting device, i.e., it is capable to record each single event retaining the energy and the interaction position (2D-sensitive detector) information of the incident photon, demonstrating to be a promising device for EDXRF imaging applications. This work presents studies of energy resolution, energy linearity and spatial resolution/elemental mapping as a function of image magnification of the system.

Keywords: Gaseous Detectors, X-ray Fluorescence, Spatial Resolution, Energy Resolution, Energy Linearity

1. Introduction

X-ray Fluorescence (XRF) techniques, including analysis and imaging are commonly used in several research fields and industrial applications. Energy Dispersive X-ray Fluorescence (EDXRF) analysis is well-known for elemental identification and quantification, while EDXRF imaging or mapping is a promising method to obtain positional distribution of specific elements in a nondestructive manner. EDXRF imaging can be used in several applications of many different fields such as geology, archaeology, electronics and life sciences [1, 2].

To obtain the elemental distribution of a sample it is necessary to use instruments that provide a precise positioning together with a good energy resolution.

Following the growing development in the area of gaseous radiation detectors, triggered by the evolving printed circuit technology, new concepts of gaseous radiation detectors emerged in the last years, namely the Micropattern Gaseous Detectors, providing new perspectives for X-ray detection and imaging [3, 4, 5]. Micro-structured charge-amplification devices opened the possibility to apply to gaseous detectors the same technology as used in semiconductor devices. Although the physical operation principle of the gaseous detectors does not allow the excellent energy resolution of the semiconductor detectors, they present important advantages such as: low cost, large detection area and single photon detection [2].

One of these structures, the 2D-Micro-Hole and Strip Plate (MHSP) has shown not only fair energy resolution capability of about 825 eV (Full-Width-at-Half-Maximum - FWHM) for 5.9 keV photons but also good spatial resolution of about 130 μm for 8 keV X-ray photons [6]. The Micro-Hole and Strip Plate [7, 8] consists on a double-sided microstructure with a Kapton$^{\text{TM}}$ foil of a 50 μm thickness, covered by a thin copper layer on both sides. On the top side, a hole pattern is etched through the microstructure and a pattern of cathode and anode strips is etched on the opposite side (bottom), both patterns are produced through a photolithography process [6]. The holes from the top side pass through the microstructure emerging in the middle of the cathode strips of the bottom side.

By applying suitable electric fields inside the holes and between anodes and cathodes, it is possible to induce two independent electron avalanches, achieving high gains: one in the holes and another one near the anode strips. The working principle of the MHSP has been already explained in detail in Refs. [7, 8].

For 2D-imaging [6], one of the dimensions is obtained by connecting the anode strips through a thin resistive layer. To obtain the second dimension, the top electrode of the MHSP is structured in strips orthogonal to the previous ones, also interconnected with a resistive line. The charge can be collected from both ends of the orthogonal resistive lines, using the principle of resistive charge division. For each dimension, it is possible to determine the centroid of the electron avalanche distribution, according to the following equation:

$$X = k\frac{X_1 - X_2}{X_1 + X_2} \quad (1)$$

where, X is the coordinate of interaction, k is a calibration factor and X_1 and X_2 are the amplitudes of the charge signals collected from both sides of the resistive layers. The energy information is obtained from the sum of the two signals collected on the same resistive line:

$$E = k(X_1 + X_2) \quad (2)$$

In the present work, we used an acquisition mode with four independent Analog-to-Digital Converters that can be time-correlated, two for each of the two resistive strips. The interaction position of the photons in the microstructure was found by applying equation 1 and the response amplitude/energy by applying equation 2, as already explained in Refs. [2, 6].

The aim of this work is to characterize the EDXRF imaging system based on a 2D-MHSP in terms of spatial and energy resolution as well as energy linearity to infer its performance in EDXRF imaging applications.

2. The EDXRF imaging system

The EDXRF imaging system is composed by an X-ray molybdenum tube (series 5000 Apogee from Oxford), a 200±8 μ m tungsten pinhole camera and a 2D-MHSP based detector arranged as shown in Figure 1(a).

The detector has an active area of about 28×28 mm^2 and allows to achieve an energy resolution of about 825 eV ($FWHM$) for 5.9 keV X-rays as well as a counting rate of up to 0.5 MHz.

For this type of imaging system, it is of major importance to use a device capable to collimate the incoming photons and focus them into the detector. The pinhole collimator, used in this work is, in fact, an aperture through which the photon must pass in order to be detected. It combines the easy manufacturing and production with the possibility of image magnification, which allows, in terms of spatial resolution, overcoming the limits imposed by the intrinsic detector response. The magnification, M, is given by the ratio of the pinhole to detector distance, d, and the pinhole to center of imaged object distance, D, as illustrated in Figure 1(b) [9].

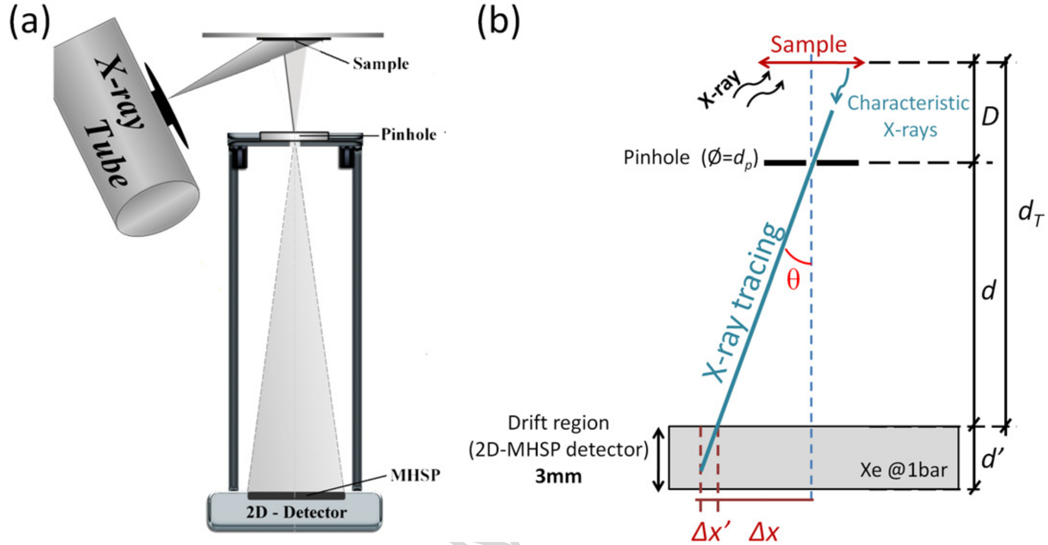

Figure 1: (a) Schematic of the proposed EDXRF imaging system, including an X-ray tube, a pinhole optics and a 2D-MHSP detector [2]. (b) A point source at a distance d_T from the detector emits a photon that passes through the pinhole, located at a distance d from detector. The photon intersects the detector plane with an incident angle θ. $\Delta x'$ is the contribution of oblique penetration of the x-ray photons in the gas medium.

In the present case the pinhole is supported by a stainless steel telescopic tube which allows to change the distance between the pinhole and the detector thus, varying the magnification of the image obtained [9]. Apart from this feature, the telescopic tube also avoids the detection of undesirable X-ray photons [2].

The fluorescence process starts when the X-rays, emitted by the X-ray tube, irradiate the sample and excite the chemical elements present on it. The characteristic fluorescence X-ray photons emitted by the elements are focused through the pinhole camera and detected in the gas volume of the 2D-detector. Once the 2D-MHSP detector is able to record both position and energy information, it is possible to obtain a map of the elements spatial distribution in the sample, by selecting the X-ray characteristic lines in the energy spectrum.

3. Spatial Resolution vs. Magnification

According to Ref. [10] the spatial resolution of a system using pinhole optics, λ_s, can be determined considering two major contributions: the intrinsic resolution of the detector, λ_i; and the contribution of the pinhole, λ_g which depends on its diameter and on the magnification, M, of the imaging system:

$$\lambda_s = \sqrt{\lambda_g^2 + \lambda_i^2} = \sqrt{d_p^2(1 + \frac{1}{M})^2 + \frac{FWHM_i^2}{M^2}} \tag{3}$$

where, d_p is the aperture diameter of the pinhole and $FWHM_i$ is the intrinsic position resolution of the detector [10]. The pinhole used in this work has a thickness of 50 μm. Its transmission is, for a photon energy of 18, 21 and 25 keV, only 4×10^{-4}, 5×10^{-3} and 4×10^{-2}, respectively. From this expression it is possible to infer the system spatial resolution as a function of the magnification.

In order to experimentally verify that assumption, a study of the spatial resolution as a function of image magnification was performed. For these studies, the present system was used, together with a 360 μm stainless steel hexagonal mesh (sample), shown in Figure 2. The edges of the hexagons had 2.8 mm long. Distances from detector-to-pinhole, d, and pinhole-to-sample, D, varied in order to get different image magnifications such as: 0.95, 1.25, 1.36, 1.64, 2.00, 2.46, 3.00 and 3.77. The acquisition time for the mesh image was typically 5 min.

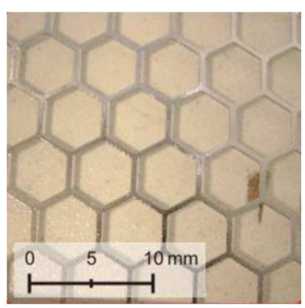

Figure 2: Sample photo: stainless steel hexagonal mesh

A summary of the obtained images are presented in Figure 3. From this figure it is possible to infer that image quality, with respect to spatial resolution, improves with image magnification.

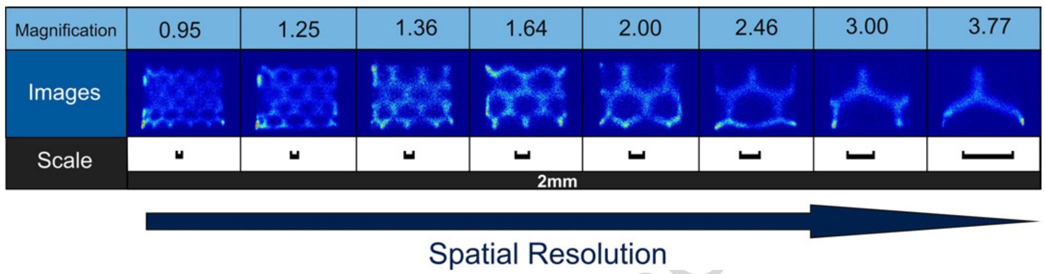

Figure 3: Image results for different magnifications

The image of the hexagonal mesh has enough information to allow the determination of position resolution of the system through the Edge Spread Function. For this, it is necessary to choose an edge being this enough for the position resolution determination. For each magnified image, a rectangle area including a region with and without the mesh edge was selected, as shown in Figure 4(a)). The obtained Edge Spread Function distribution was fitted to a sigmoid function (Figure 4(b)). The Full-Width-at-Half-Maximum of the fitting function (Line Spread Function) is related to the system spatial resolution [11].

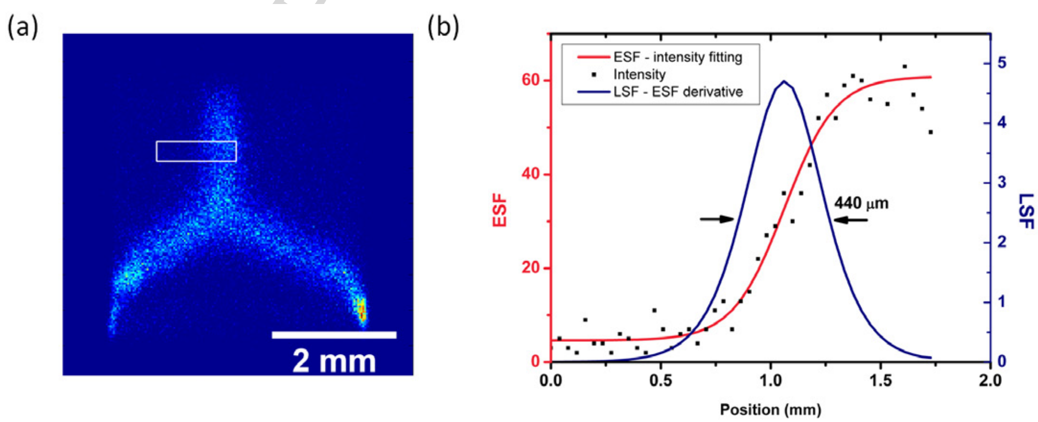

Figure 4: (a)Fluorescence image of the hexagonal mesh with a magnification of 3.77. The selected region for spatial resolution calculations is delimited with a white rectangle. (b)Edge Spread Function (ESF) and Line Spread Function (LSF) used to determine the position resolution.

The Modular Transfer Function (MTF) represents the spatial frequency response of an imaging system. This function describes how the imaging system behaves in the spatial frequency domain, being calculated through the Fourier transform of the Line Spread Function [11]. In the present work, we describe the system position resolution using the spatial frequency where the MTF is reduced to 3%, a value related with the human eye ability to distinguish low contrast differences in an image [11]. As an example, the MTF shows a resolution of 2.4 lp/mm (lines-pair per millimeter) at an amplitude of 3% for the image with higher magnification as illustrated on Figure 5.

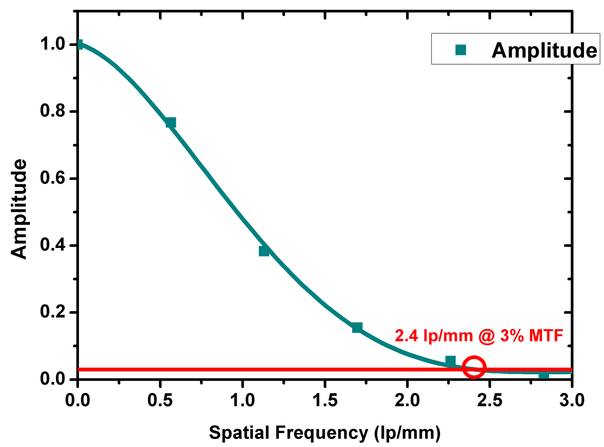

Figure 5: Modulation transfer function (MTF) of the region marked in the image of the Figure 4(a)

Figure 6 shows the Modular Transfer Function for all the acquired magnified images. As can be seen, the spatial frequency increases with the increase of magnification, meaning that the spatial resolution of the system is better for higher magnification values, in agreement with equation 3.

In Figure 7, the FWHM of the Line Spread Function is presented as a function of magnification. It is also presented the predicted theoretical curves from equations 3 and 4.

Taking into account the oblique penetration and the different depth of interaction of X-rays along the detector drift region (illustrated in Figure 1(b)), an uncertainty $\Delta x'$ needs to be added as a contribution to equation 3, which is represented by the third term of the following equation:

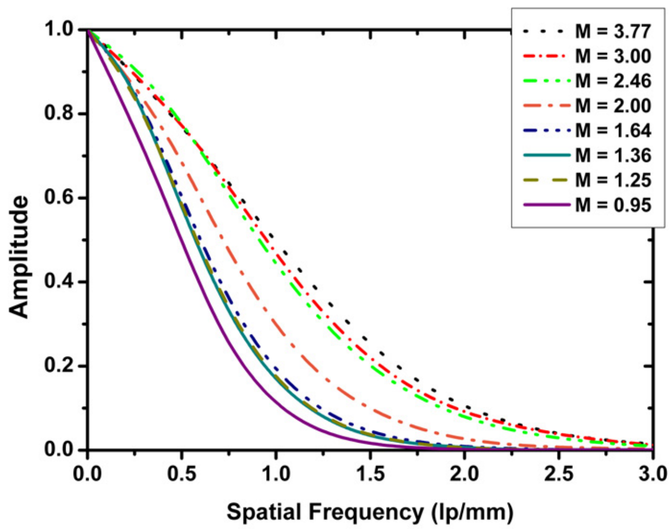

Figure 6: Modular transfer function for the images obtained for different magnifications

$$\lambda_s = \sqrt{\lambda_g^2 + \lambda_i^2 + \lambda_{\Delta x'}^2}$$

$$\Leftrightarrow \lambda_s = \sqrt{d_p^2(1+\frac{1}{M})^2 + \frac{FWHM_i^2}{M^2} + \frac{(d'\Delta x/d_T)^2}{M^2}(1+\frac{1}{M})^2} \quad (4)$$

Thus, the equation 4 takes into account not only with the contribution of the intrinsic resolution of the detector, λ_i, and with the contribution of the pinhole, λ_g, but also with the contribution of the oblique penetration of the X-rays along the detector drift region, $\lambda_{\Delta x'}$. This dependence (Eqn. 4) is plotted in Figure 7. This plot shows that the contribution of the X-ray photons oblique penetration is small and can be considered negligible for highest magnification values. The calculations for this contribution were made to a value of Δx close to window limits which means that the curve obtained corresponds to the worst possible situation. The experimental system spatial resolution ($FWHM$) varies between 900 and 400 μm for an image magnification between about 1 and 4. Both, experimental and theoretical predictions present the same trend and experimental curves approaches the theoretical one for higher values of M. Nevertheless, position resolutions obtained for the experimental data are little worse than the theoretical values, possibly due to some non-uniformities of the sample, the pinhole, and the detector.

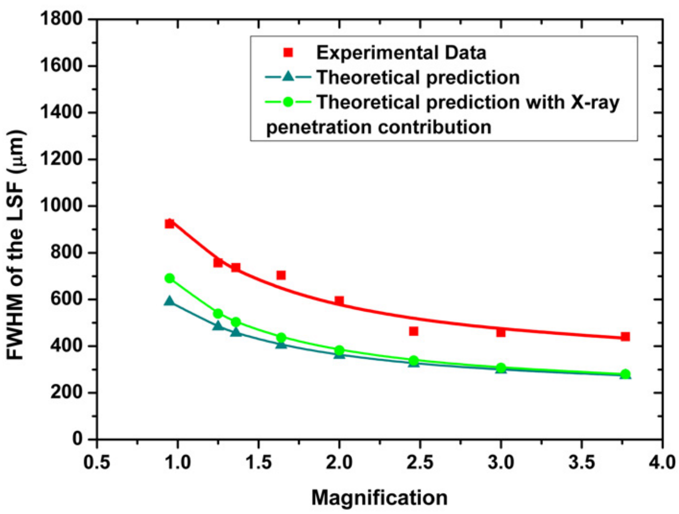

Figure 7: $FWHM$ of the Line Spread Function as a function of magnification: comparison between experimental and theoretical predictions

According to equation 3 and 4, the intrinsic resolution of the detector is more significant for lower values of magnification.

Note also that the spatial resolution saturates to a value close to pinhole diameter (Figure 7). This means that the pinhole diameter limits the spatial resolution of the system, even if we further increase the image magnification or/and the detector position resolution. To reach higher spatial resolutions, it is mandatory to use a pinhole with a smaller aperture. By reducing the pinhole diameter it is possible to further improve the system imaging resolution, however it will produce a quadratic reduction of the pinhole efficiency [10]. Thus, it is necessary to establish a compromise between the spatial resolution and the detection efficiency of the system.

4. Energy linearity and Energy Resolution

The energy linearity of the EDXRF system was determined for X-ray photons within an energy range between 3 and 25 keV. Fluorescence radiation was obtained by irradiation of different single-element targets including pure elements, oxides or salts, such as: Ca, V, Cr, Mn, Fe, Co, Ni, Cu, Zn, Ge, Zr, Mo, Pd e Sn. The time of acquisition was typically 30s. As an example, the Cu and Mo K-lines spectra can be seen on Figure 8.

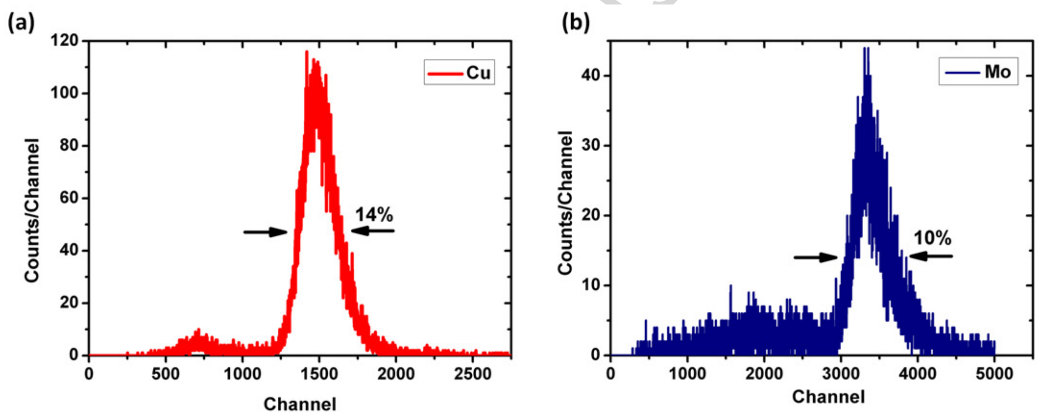

Figure 8: Pulse height distributions of K-lines from: (a) Cu and; (b) Mo

During acquisitions, the sample-to-detector distance was typically 20 cm. The detector window was coupled to a lead collimator containing a hole with 2 mm diameter. Fluorescence radiation was induced by X-rays from the X-ray tube by using different currents and voltages depending on the analyzed sample.

In Figure 9(a) the pulse amplitude (the centroid of the peak distribution) and the energy resolution values of the measured pulse-height distributions are plotted as a function of X-ray energy. As expected, good energy linearity is maintained throughout the measured energy range. The energy resolution shows also a reasonable linearity with $E^{-1/2}$, as illustrated in Figure 9(b).

Although energy resolution behaves as expected, the obtained values are still worse than the intrinsic energy resolution of the detector. It is known that the amplitude response as a function of interaction position in the detector is not a constant value for monochromatic radiation photons. This is due to the different response along the microstructure because of

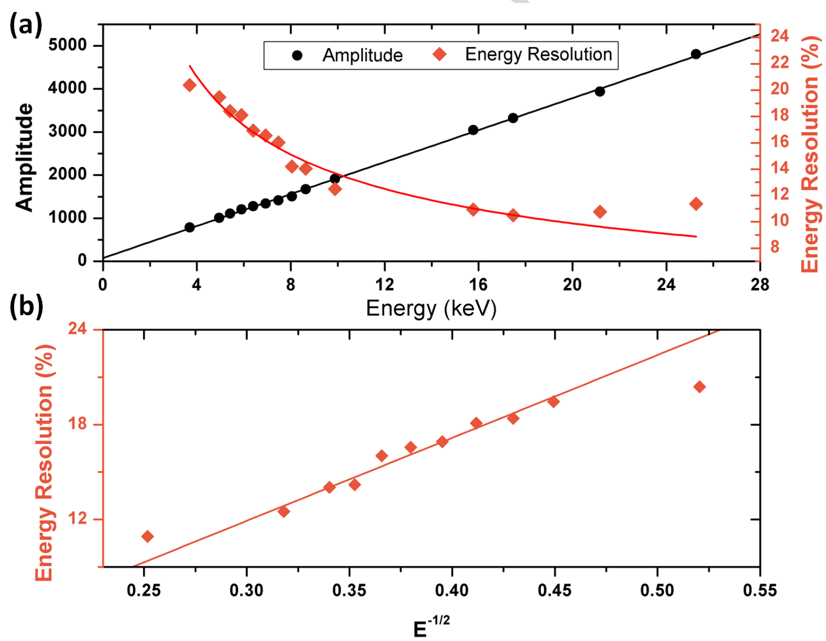

Figure 9: (a)Pulse amplitude and energy resolution as a function of X-ray energy; (b)Energy resolution as a function of the inverse of square root of the X-ray energy.

the non-uniformities resulting from the fabrication process and leads to a deterioration of energy resolution. To overcome this problem an amplitude correction method was developed, which was explained in detail in Ref. [2].

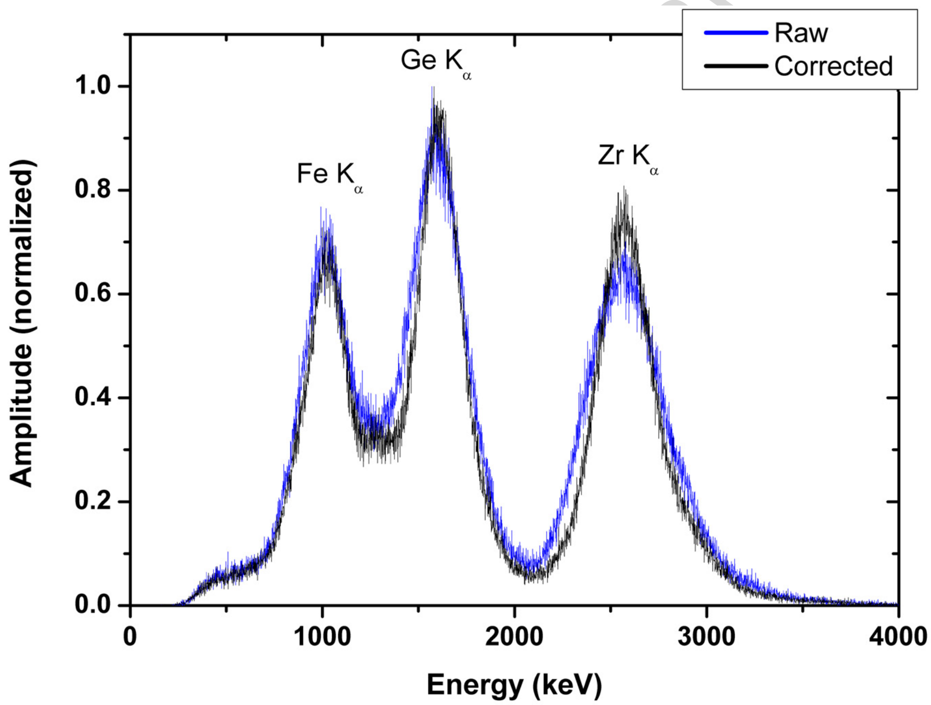

Figure 10: Raw and corrected pulse height distributions from a Fe, Ge and Zr sample

As can be seen in Figure 10, the correction method gives a clear improvement in the energy resolution and on the shape of fluorescence spectrum of the three-element sample example. For an energy of 9.89 and 15.77 keV, an improvement in the energy resolution of 17% and 24%, respectively, was obtained in comparison with the non-corrected one. This spectrum was obtained irradiating the whole active area of the detector.

A spectrum was also acquired by direct irradiation of the detector with an ^{241}Am γ source to evaluate the detector energy dynamic range, Figure 11. The spectral features include the fluorescence L-lines from Neptunium (respectively 13.95, 17.74 and 20.78 keV), the 59.6 keV peak from ^{241}Am γ-rays and other fluorescence lines associated with the experimental setup (Pb from the collimator and Xe escape lines). The spectrum shows clearly the detector intrinsic high energy dynamic range.

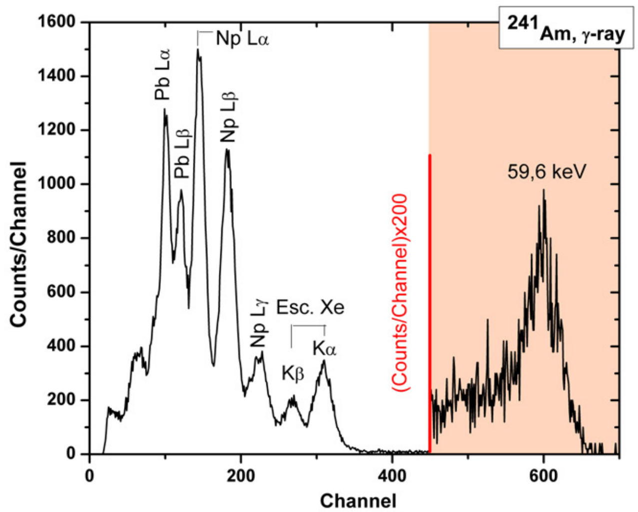

Figure 11: ^{241}Am pulse-height distribution

5. Conclusions

The performance characteristics of the energy dispersive X-ray fluorescence imaging system based on a 2D-MHSP detector, filled with Xe at 1 bar, have been presented.

The spatial resolution of the system was determined as a function of image magnification due to the use of pinhole optics. As expected the increase of image magnification improves the spatial resolution. Spatial resolution ($FWHM$) of the experimental system varied between 900 and 400 μm for image magnifications between 1 and 4. The contribution of oblique penetration of X-ray photons was found to be negligible for high values of magnification. Future work will include the increase of the spatial resolution by using a pinhole with a smaller aperture.

Energy resolution and linearity, in the 3-25 keV X-ray energy range were determined from the pulse-height distributions of the fluorescence X-ray spectra induced in a variety of single- and multi-element sample materials.

The energy resolution have shown good linearity with the inverse of the square root of the X-ray energy.

Future development work will focus also on the improvement of the gas purification in order to further improve the energy resolution, by using getters coupled to the detector; and on the improvement of the detection efficiency by increasing the drift region and/or the gas pressure; as well as the increase of the effective area of the detector.

Acknowledgements

This work was partially supported by project CERN/FP/109283/2009. A.L.M. Silva, C.D.R. Azevedo and C.A.B. Oliveira were supported by a doctoral grant from FCT (Lisbon) with the respective references, SFRH/BD/61862/2009, SFRH/BD/35979/2007, SFRH/BD/36562/2007 .

References

[1] A. L. M. Silva, C. A. B. Oliveira, A. L. Gouvêa, J. M. F. dos Santos, M. L. Carvalho, J. F. C. A. Veloso, EDXRF imaging of Pb in glazed ceramics using a micropattern gas detector, Anal. and Bioanal. Chem. 395 (2009) 2073–2080.

[2] J. F. C. A. Veloso, A. L. M. Silva, C. A. B. Oliveira, A. L. Gouvêa, C. D. R. Azevedo, L. Carramate, H. N. da Luz, J. M. F. dos Santos, Energy resolved x-ray fluorescence imaging based on a micropattern gas detector, Spectrochim. Acta, Part B 65 (2010) 241–247.

[3] J. F. C. A. Veloso, J. M. F. dos Santos, C. A. N. Conde, R. Morgado, Application of a Microstrip Gas Counter in Energy Dispersive X-ray Fluorescence Analysis, X-Ray Spectrom. 26 (1997) 237–243.

[4] F. Sauli, A. Sharma, Micropattern gaseous detectors, Annu. Rev. of Nucl. and Part. Sci. 49 (1999) 341–388.

[5] L. Shekhtman, Micro-pattern gaseous detectors, Nucl. Instrum. Methods Phys. Res., Sect. A 494 (2002) 128–141.

[6] H. N. da Luz, C. A. B. Oliveira, C. D. R. Azevedo, J. A. Mir, R. d. Oliveira, J. M. F. dos Santos, J. F. C. A. Veloso, Single photon counting x-ray imaging system using a Micro-Hole and Strip Plate, IEEE Trans. Nucl. Sci. Symposium Conference Record 55 (2008) 2341–2345.

[7] J. F. C. A. Veloso, J. M. F. dos Santos e C. A. N. Conde, A proposed new microstructure for gas radiation detectors: The Micro-Hole-and-Strip Plate (MHSP), Rev. Sci. Instrum. 71 (2000) 2371–2376.

[8] M. Maia, J. F. C. A. Veloso, J. M. F. dos Santos, A. Breskin, R. Chechik, D. Möermann, Advances in the Micro-Hole and Strip Plate gaseous detector, Nucl. Instrum. Methods Phys. Res., Sect. A 504 (2003) 364–368.

[9] G. F. Knoll, Radiation detection and measurement, 3rd Edition, John Wiley & Sons, New York, 2000.

[10] R. Accorsi, S. D. Metzler, Analytic determination of the resolution-equivalent effective diameter of a pinhole collimator, IEEE Trans. Med. Imaging 23 (2004) 750–763.

[11] S. W. Smith, The Scientist and Engineer's Guide to Digital Signal Processing, second edition Edition, California Technical Publishing, 1999.